Int J Clin Exp Med 2015;8(7):10687-10695
www.ijcem.com /ISSN:1940-5901/IJCEM0009123

*Original Article*

# Design and finite element analysis of a novel sliding rod microscrew implantation device for mandibular prognathism

Yanfeng Li[1*], Yuan Lv[2*], Yongjin Lu[3], Pan Zeng[3], Xianglong Zeng[4], Xiaoqian Guo[1], Weili Han[1]

*[1]Department of Stomatology, First Affiliated Hospital of Peoples Liberation Army General Hospital, Beijing, China; [2]Master's Training Site, First Affiliated Hospital of Peoples Liberation Army General Hospital, Liaoning Medical Universiy, Liaoning, China; [3]Department of Mechanical Engineering, Tsinghua University, Beijing, China; [4]Department of Orthodontics, School of Stomatology of Peking University, Beijing, China. [*]Equal contributors.*

Received April 15, 2015; Accepted July 6, 2015; Epub July 15, 2015; Published July 30, 2015

**Abstract:** Tooth distalization is an effective approach for mandibular prognathism. Current distalization devices are bulky and clinically complicated. Here, we designed a novel molar distalization device by using a sliding rod and a microscrew and performed a mechanical analysis and finite element model (FEM) analysis of force distribution and displacement of the upper canine, first and second premolar and first molar. A 2D FEM was constructed using the Beam3 element and a 3D FEM was constructed of the mandibular teeth, the periodontal membrane, and the alveolar bones using the UG software. The upper first molar was divided into 12 points on the dental surface to facilitate stress analysis. Force analysis using the ANSYS WORKBECNH revealed that, both horizontally and vertically, the traction force causing distalization of the first molar decreased when the spring coil moved down the L shaped sliding rod. The 3D FEM force analysis revealed distomedial displacement of the upper first molar when the sliding rod microscrew implantation device caused distalization of the molar. These findings support further exploration for the use of the sliding rod microscrew implants as an anchorage for group distal movement of the teeth of patients with mandibular prognathism.

**Keywords:** Mandibular prognathism, molar, distalization, microscrew, finite element analysis

## Introduction

Mandibular prognathism is predominantly class II and often manifested as crowding of teeth [1, 2]. Its treatment frequently requires distomedial displacement of the mandibular tooth, including distomedial displacement of the front and back teeth or group distomedial displacement [3]. Tooth distalization is an effective approach for mandibular or bimaxillary prognathism. Currently, multiple tooth distalization devices are in use clinically [4].

Mandibular group distalization can be done by molar distalization first and then premolar distalization. Most studies focus on devices for molar distalization. Patient-dependent molar distalization devices require cooperation of patients [5]. The use of microscrew implant to provide anchorage for distalization of molar has been actively pursued by investigators [6] in order to obtain a device that is simple in design and clinically easy to maneuver with good controllability, sustained force release, and reliable anchorage. Park et al. [7] used microscrew implants between the second premolar and first molar and achieved distalization of the mandibular teeth after one year, which, however, was restrained by the microscrews. Kyung et al. [8] used a modified procedure by removing the microscrew implant after achieving distalization of the second molar and then re-implanted microscrews to realize group distalization, markedly increasing the cost and complexity of the procedure. These devices and others are bulky in volume and cause foreign body sensation. The distalization is also rather limited and the procedure is clinically complicated and time consuming.

We designed a novel molar distalization device by using a sliding rod and a microscrew.

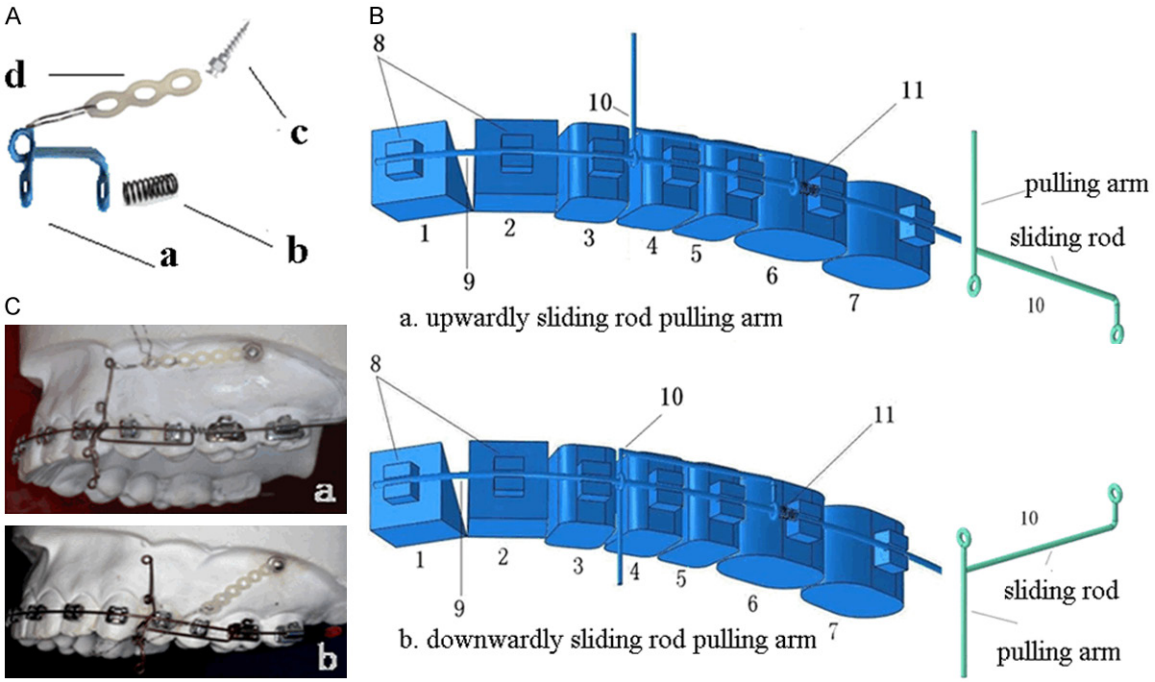


**Figure 1.** The sliding rod microscrew implantation device. A. Photograph of the actual sliding rod microscrew implantation device. a, sliding rod, b, nickel titanium spring, c, microscrews and d, spring coil. B. Schematic representation of the implantation device with the traction bar turning upward or downward. 1 to 7: mandibular teeth; 8: bracket; 9: archwire; 10, L-shaped sliding rod; 11, nickel titanium spring; 12, microscrew; 13, elastic wire ring. C. Application of the sliding rod microscrew implantation device.

Theoretically, it can ease crowding of teeth without the needs of tooth extraction and at the same time maintain the stability of the oromaxillary system. The sliding rod microscrew implantation device causes distalization of a molar as well as distalization of the mandibular group. Finite element analysis can solve structural mechanical problems and is used in dentistry to determine the behavior parameters in response to loading complex structures [9-12]. In the current study, we carried out a mechanical analysis and finite element model (FEM) analysis of force distribution and displacement of the upper canine, first and second premolar and first molar. The finite element analysis and mechanical analysis of the sliding rod microscrew implantation device may provide data to guide further optimization of the device for clinical use.

## Materials and methods

### *The sliding rod microscrew implantation device*

The sliding rod microscrew implantation device included an L-shaped sliding rod, nickel titanium spring, microscrews and spring coil. Each tooth was connected with the archwire via a bracket (**Figure 1**). The microscrew was 1.2 to 2 mm in diameter and 10 to 12 mm in length and was first inserted at a depth of 1 to 1.5 mm vertical to and then at an angle of 55 to 70 degree to the mandibular plane into the bony area of the infrazygomatic crest above the mucogingival junction near the mesiobuccal root of the upper second molar. One end of the spring coil was connected to the microscrew, and the steel wire was tied to the traction bar of the L-shaped sliding rod. The traction bar can be turned upward towards the gingival or downward.

### *The 2D finite element model of the sliding rod microscrew implantation device*

A 2D FEM was constructed of molar distalization with the sliding rod microscrew implantation device using the Beam3 element. The composite structures were analyzed in ANSYS (version 13.0) Mechanical APDL. At the hinge joint of the sliding rod and the archwire, coupling restraint was applied for displacement at point

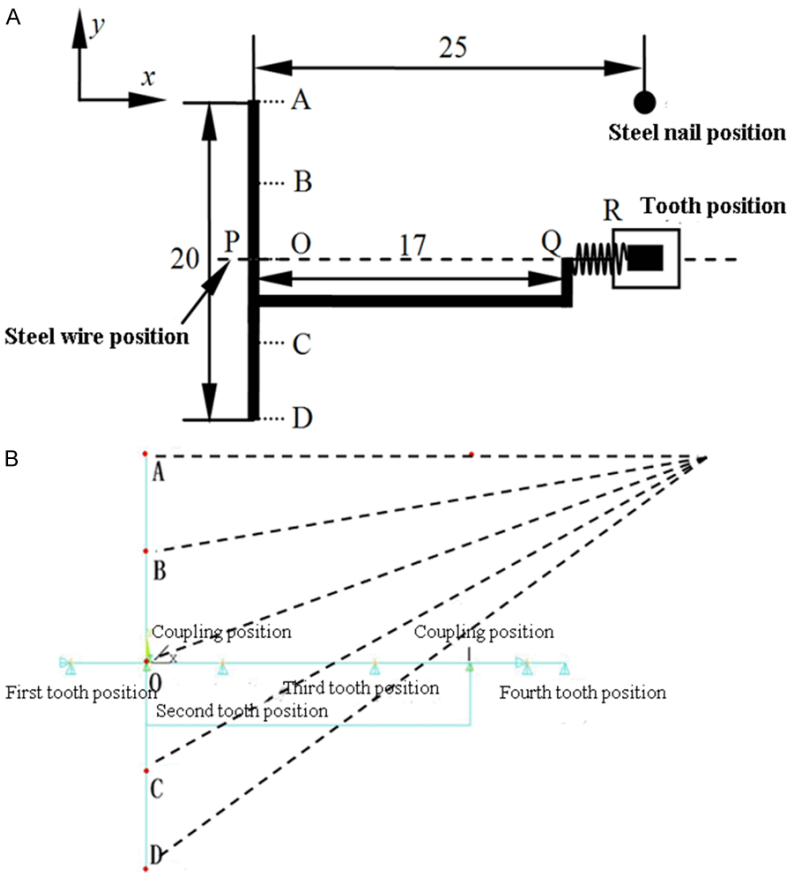


**Figure 2.** A. Design of the sliding rod microscrew implantation device. B. Two dimensional (2D) finite element model (FEM) of the device.

O and Y axis to model the sliding and hinging of the archwire (**Figure 2A**). Displacement restraint for total degree of freedom was applied at the upper canine, first and second premolar and first molar, and the end of the spring coil (**Figure 2B**). A load of 1.5N was applied and the origin of force was A, B, O, C, and D. The mechanical force in the x and y axis of the upper tooth canine, first and second premolar and first molar was calculated.

*The 3D FEM for the upper first molar*

A 3D FEM was constructed of the mandibular teeth, the periodontal membrane, and the alveolar bones using the UG software. The second order 10-node modified quadratic tetrahedral solid elements (C3D10M) in ABAQUS were used for meshing. Displacement restraint was applied for horizontal and axial movement of the alveolar bones. Load restraint was applied for the surface of the buccal tube for bonding whose force area was 7.34 $mm^2$ in the shape of an isosceles trapezoid with the top base (the gingival surface) at 3.2 mm and the bottom base (the occlusal surface) at 4 mm at a height of 2.04 mm. At a load of 1.5 N, the corresponding pressure intensity was 0.20 Mpa (**Figure 3**). The upper first molar used in this work was divided into 12 points on the dental surface to facilitate the analysis of the stresses (**Figure 4**). Loading force was transmitted to the whole tooth via the base of the buccal tube of the upper first molar. The von Mises stress, maximal and minimal principal stress, displacement along x, y, and z axis were determined by the origin of force and $x^2+y^2+z^2$ was calculated. The point close to the center of rotation was identified and the movement of the upper first molar was observed.

*Material properties*

The archwire and sliding rod were steel and had an elastic modulus of 210 GPa (1, 2.1E5) and a Poisson's ratio of 1, 0.29, and a density of 1, 7.8e-9. Tooth and alveolar bones were presumed to be homogeneous, isotropic and linearly elastic material. Teeth had an elastic modulus of 19600 MPa and a Poisson's ratio of 0.3. Alveolar bones had an elastic modulus of 14700 MPa and a Poisson's ratio of 0.28. The periodontal membrane had an elastic modulus of 3 MPa and a Poisson's ratio of 0.45 [11].

## Results

*2D FEM force analysis*

The number of finite elements was 210 in the 2D FEM of the sliding rod microscrew implantation device. A load of 1.5N was separately applied to the anchorage site A, B, O, C, and D (**Figure 2B**). The force distribution at the upper tooth canine, first and second premolar and first molar in the direction of x and y axis is shown in **Table 1** and the data of mechanical

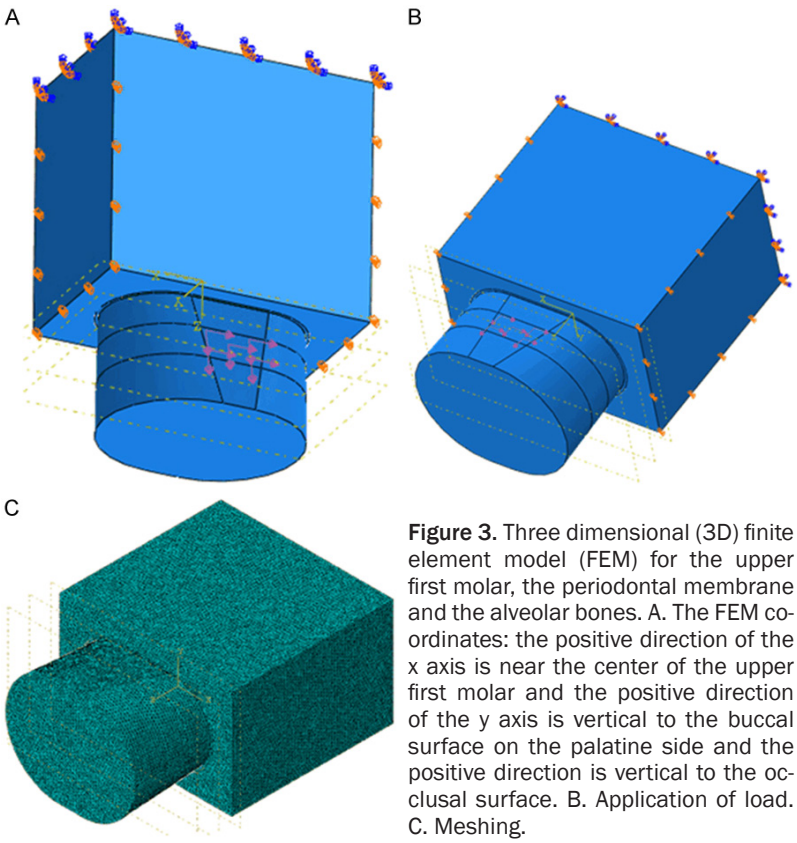


**Figure 3.** Three dimensional (3D) finite element model (FEM) for the upper first molar, the periodontal membrane and the alveolar bones. A. The FEM coordinates: the positive direction of the x axis is near the center of the upper first molar and the positive direction of the y axis is vertical to the buccal surface on the palatine side and the positive direction is vertical to the occlusal surface. B. Application of load. C. Meshing.

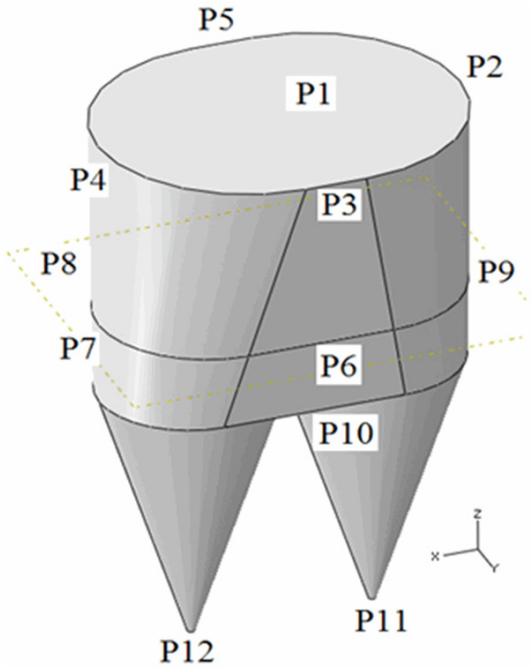


**Figure 4.** The parameters of the upper first molar, the periodontal membrane and the alveolar bones in the 3D FEM.

force analysis are shown in **Table 2**. The deformation map in the direction of x and y axis and axial force distribution map in the FEM were obtained and are shown in **Figure 1**. Force analysis of the upper canine, first and second premolar and first molar using the ANSYS WORKBECNH revealed that, both horizontally and vertically, the traction force causing distalization of the first molar decreased when the spring coil moved down the L shaped sliding rod from the anchorage site A to D (**Table 1**). When the vertical load was separately applied to the anchorage site A, B, or O, the upper canine and the first premolar experienced a downward force while the upper second premolar and the first molar experienced a stretching force. Furthermore, the upper occlusal plane showed a tendency for counterclockwise rotation, which was weakened when the origin of force changed from A to D. When the origin of force moved from O to D, the downward force on the upper canine and first premolar was further weakened and the upper second premolar and first molar experienced an increasing downward force. Additionally, the mandible exhibited a trend for switch to clockwise rotation from counterclockwise rotation. Mechanical force analysis of the upper canine, first and second premolar and first molar showed similar results to force analysis using the ANSYS program (**Table 2**).

*3D FEM force analysis*

The number of elements in the 3D FEM for the upper first molar was 1271576 and the number of nodes was 1834875. The upper first molar had 396635 elements and 553132 nodes; the periodontal membrane had 212848 elements and 355732 nodes. The alveolar bones had 662093 elements and 926011 nodes (**Figure 3**). When the origin of force changed from A to D, the values on the x axis for the 12 points on the surface of the upper first molar were all negative except P11 and P12, indicating distomedial displacement of the upper first molar when the sliding rod microscrew implantation

**Table 1.** Force analysis of the upper canine, first and second premolar and first molar using the ANSYS WORKBECNH Version 13.0

| Position / Force (N) / Origin of force | Total load | | Canine | | Fist premolar | | Second premolar | | Fist molar | |
|---|---|---|---|---|---|---|---|---|---|---|
| | Fx | Fy | R3x | R3y | R4x | R4y | R5x | R5y | R6x | R6y |
| A | 1.50 | 0.00 | 0 | 0.65 | 0 | 0.65 | 0 | -0.87 | 1.50 | -0.44 |
| B | 1.47 | 0.29 | 0 | 0.52 | 0 | 0.52 | 0 | -0.61 | 1.47 | -0.14 |
| O | 1.39 | 0.56 | 0 | 0.38 | 0 | 0.38 | 0 | -0.35 | 1.39 | 0.14 |
| C | 1.29 | 0.77 | 0 | 0.25 | 0 | 0.25 | 0 | -0.12 | 1.29 | 0.39 |
| D | 1.17 | 0.94 | 0 | 0.14 | 0 | 0.14 | 0 | 0.08 | 1.17 | 0.58 |

**Table 2.** Mechanical force analysis of upper canine, first and second premolar and first molar

| Position / Force (N) / Origin of force | Total load | | Canine | | First premolar | | Second premolar | | First molar | |
|---|---|---|---|---|---|---|---|---|---|---|
| | Fx | Fy | R3x | R3y | R4x | R4y | R5x | R5y | R6x | R6y |
| A | 1.50 | 0.00 | 0.00 | 0.44 | 0.00 | 0.44 | 0.00 | -0.44 | 1.50 | -0.44 |
| B | 1.47 | 0.29 | 0.00 | 0.36 | 0.00 | 0.36 | 0.00 | -0.22 | 1.47 | -0.22 |
| O | 1.39 | 0.56 | 0.00 | 0.28 | 0.00 | 0.28 | 0.00 | 0.00 | 1.39 | 0.00 |
| C | 1.29 | 0.77 | 0.00 | 0.20 | 0.00 | 0.20 | 0.00 | 0.19 | 1.29 | 0.19 |
| D | 1.17 | 0.94 | 0.00 | 0.12 | 0.00 | 0.12 | 0.00 | 0.35 | 1.17 | 0.35 |

**Table 3.** Force and displacement at 12 points of the left first molar when the load is applied at the origin of force A

| | von Mises stress (MPa) | Maximal principal stress (MPa) | Minimal principal stress (MPa) | Displacement in x axis (mm) | Displacement in y axis (mm) | Displacement in z axis (mm) | $x^2+y^2+z^2$ |
|---|---|---|---|---|---|---|---|
| P1 | 0.031457 | 0.016375 | -0.019899 | -0.001584 | 0.00011 | 0.000197 | 2.56E-06 |
| P2 | 0.007111 | 0.006888 | -0.000365 | -0.001597 | -0.00064 | 0.00131 | 4.681E-06 |
| P3 | 0.00882 | 0.007607 | -0.002075 | -0.002025 | 0.000143 | 0.000232 | 4.175E-06 |
| P4 | 0.009418 | 0.00018 | -0.009317 | -0.001576 | 0.000927 | -0.00101 | 4.365E-06 |
| P5 | 0.004968 | 0.00412 | -0.001423 | -0.001148 | 0.000108 | 0.000123 | 1.344E-06 |
| P6 | 0.184851 | 0.115711 | -0.097559 | -0.001041 | 8.8E-05 | 0.000134 | 1.109E-06 |
| P7 | 0.062625 | -0.01071 | -0.079654 | -0.000699 | 0.000792 | -0.00101 | 2.139E-06 |
| P8 | 0.092373 | 0.047785 | -0.058671 | -0.000406 | 3.86E-05 | 9.74E-05 | 1.755E-07 |
| P9 | 0.074761 | 0.092809 | 0.0126234 | -0.000743 | -0.00071 | 0.001307 | 2.77E-06 |
| P10 | 0.169151 | 0.167872 | -0.130351 | -0.00037 | 1.23E-06 | 0.00015 | 1.592E-07 |
| P11 | 0.278257 | 0.031919 | -0.142675 | 0.0005094 | -0.0002 | 0.000716 | 8.132E-07 |
| P12 | 0.183749 | 0.026186 | -0.108433 | 0.0005113 | 4.67E-05 | -0.00042 | 4.386E-07 |

device caused distalization of the molar (**Tables 3-7**). When the origin of force changed from A to D, P4, P7, and P12 on the y axis were positive, suggesting movement towards the palatal tooth surface. P2, P9, and P11 remained negative all the time, suggesting movement toward the buccal surface. Furthermore, the absolute displacement inP3x was > the absolute displacement in P5x. In addition, $P3_{\text{von Mises stress}}$ was > $P5_{\text{von Mises stress}}$. Moreover, P10 was the nadir of displacement in $x^2+y^2+z^2$ followed by P8, indicating that P10 at the branching point of the root of the molar was closer to the center of rotation.

## Discussion

In the current study, we designed a novel sliding rod microscrew implantation device. The upper canine, first and second premolar are stabilized by the steel wire while the first and

**Table 4.** Force and displacement at 12 points of the left first molar when the load is applied at the origin of force B

| | von Mises stress (MPa) | Maximal principal stress (MPa) | Minimal principal stress (MPa) | Displacement in x axis (mm) | Displacement in y axis (mm) | Displacement in z axis (mm) | $x^2+y^2+z^2$ |
|---|---|---|---|---|---|---|---|
| P1 | 0.030275 | 0.016463 | -0.01847 | -0.00155 | 3.97E-05 | 0.000119 | 2.429E-06 |
| P2 | 0.007654 | 0.007489 | -0.00036 | -0.00154 | -0.0007 | 0.001208 | 4.334E-06 |
| P3 | 0.007419 | 0.005543 | -0.00286 | -0.00199 | 7.12E-05 | 0.000114 | 3.961E-06 |
| P4 | 0.008659 | 0.000187 | -0.00856 | -0.00155 | 0.00084 | -0.00106 | 4.224E-06 |
| P5 | 0.004418 | 0.003293 | -0.00172 | -0.00113 | 3.79E-05 | 8.36E-05 | 1.276E-06 |
| P6 | 0.182196 | 0.109777 | -0.10051 | -0.00102 | 3.59E-05 | 7.77E-05 | 1.049E-06 |
| P7 | 0.066415 | -0.01192 | -0.08427 | -0.00071 | 0.00076 | -0.00106 | 2.202E-06 |
| P8 | 0.082189 | 0.043934 | -0.05086 | -0.00042 | 5.55E-06 | 7.15E-05 | 1.809E-07 |
| P9 | 0.068479 | 0.075929 | 0.00401 | -0.00074 | -0.00072 | 0.001207 | 2.525E-06 |
| P10 | 0.165321 | 0.167239 | -0.12592 | -0.00036 | 8.18E-07 | 7.34E-05 | 1.368E-07 |
| P11 | 0.272361 | 0.031033 | -0.1371 | 0.0005 | -0.00016 | 0.000629 | 6.719E-07 |
| P12 | 0.179451 | 0.025729 | -0.10444 | 0.000501 | 8.19E-05 | -0.00048 | 4.901E-07 |

**Table 5.** Force and displacement at 12 points of the left first molar when the load is applied at the origin of force O

| | von Mises stress (MPa) | Maximal principal stress (MPa) | Minimal principal stress (MPa) | Displacement in x axis (mm) | Displacement in y axis (mm) | Displacement in z axis (mm) | $x^2+y^2+z^2$ |
|---|---|---|---|---|---|---|---|
| P1 | 0.02269 | 0.01288 | -0.01331 | -0.00147 | -1.85E-05 | 2.64E-05 | 2.17E-06 |
| P2 | 0.00615 | 0.00604 | -0.00025 | -0.00146 | -0.000492 | 0.000673 | 2.83E-06 |
| P3 | 0.00528 | 0.00301 | -0.00306 | -0.00188 | 1.23E-06 | 2.64E-07 | 3.54E-06 |
| P4 | 0.00611 | 0.00015 | -0.00603 | -0.00146 | 0.0004943 | -0.00067 | 2.84E-06 |
| P5 | 0.00317 | 0.002 | -0.00163 | -0.00107 | -1.93E-05 | 2.78E-05 | 1.14E-06 |
| P6 | 0.13983 | 0.08247 | -0.07892 | -0.00097 | -9.24E-06 | 1.39E-05 | 9.35E-07 |
| P7 | 0.05676 | -0.0084 | -0.06913 | -0.00071 | 0.0004726 | -0.00067 | 1.17E-06 |
| P8 | 0.06182 | 0.03491 | -0.03644 | -0.0004 | -9.19E-06 | 1.41E-05 | 1.58E-07 |
| P9 | 0.0547 | 0.06699 | 0.007972 | -0.00069 | -0.000473 | 0.000671 | 1.15E-06 |
| P10 | 0.65546 | 0.10684 | -0.1116 | -0.00035 | -7.37E-07 | 1.56E-06 | 1.22E-07 |
| P11 | 0.15674 | 0.02326 | -0.02507 | 0.000474 | -8.10E-05 | 0.00033 | 3.40E-07 |
| P12 | 0.13489 | 0.0195 | -0.03537 | 0.000474 | 7.57E-05 | -0.00033 | 3.38E-07 |

second molar can slide freely along the wire via the buccal tube. The medioproximal sliding arm of the L-shaped sliding rod is positioned between the upper canine and first premolar and is close to the upper canine. The mediodistal sliding arm of the L-shaped sliding rod is positioned between the upper second premolar and the first molar and is close to the second premolar. The nickel titanium spring is positioned between the mediodistal sliding arm of the L-shaped sliding rod and the medioproximal first molar. It stretches the elastic wire ring and generates a traction force that acts on the traction bar of the L-shaped sliding rod, which transmits the horizontal traction force posteriorly to the mediodistal sliding arm of the L-shaped sliding rod and thereby compresses the nickel titanium spring. The latter stores and releases in a sustained manner the horizontal force, causing distalization and mediodistal displacement along the wire of the first (and second) molar. A gap is created between the upper second premolar and the first molar. When the device is used unilaterally, it causes the distalization of the molar and when it is used bilaterally, it causes traction of the bilateral molars. If the left upper second molar to the right upper second molar are stabilized by the steel wire, the device causes group distalization of the upper mandibular teeth. Group distalization can be realized using microscrew implants in one step [7] or first by molar distalization followed by front tooth distalization [8]. Our device can achieve front tooth distalization, molar dis-

**Table 6.** Force and displacement at 12 points of the left first molar when the load is applied at the origin of force C

| | von Mises stress (MPa) | Maximal principal stress (MPa) | Minimal principal stress (MPa) | Displacement in x axis (mm) | Displacement in y axis (mm) | Displacement in z axis (mm) | $x^2+y^2+z^2$ |
|---|---|---|---|---|---|---|---|
| P1 | 0.027382 | 0.016099 | -0.01551 | -0.00134 | -8.4E-05 | -2.5E-05 | 1.793E-06 |
| P2 | 0.00773 | 0.007613 | -0.00021 | -0.00133 | -0.00073 | 0.00093 | 3.172E-06 |
| P3 | 0.006931 | 0.001943 | -0.00572 | -0.00174 | -8.7E-05 | -5.9E-05 | 3.025E-06 |
| P4 | 0.006609 | 0.000203 | -0.0065 | -0.00135 | 0.000616 | -0.00106 | 3.32E-06 |
| P5 | 0.003709 | 0.001862 | -0.00237 | -0.00098 | -8.6E-05 | 8.99E-06 | 9.76E-07 |
| P6 | 0.160502 | 0.083113 | -0.10192 | -0.00089 | -3E-06 | -0.00011 | 8.08E-07 |
| P7 | 0.05794 | -0.01199 | -0.07473 | -0.00062 | 0.000631 | -0.00106 | 1.894E-06 |
| P8 | 0.071576 | 0.042556 | -0.04004 | -0.00037 | -3E-05 | -2.1E-05 | 1.356E-07 |
| P9 | 0.066063 | 0.079758 | 0.00894 | -0.00065 | -0.00066 | 0.00092 | 1.711E-06 |
| P10 | 0.143823 | 0.15104 | -0.16867 | -0.00032 | 3.66E-08 | -6.5E-05 | 1.047E-07 |
| P11 | 0.237734 | 0.026851 | -0.02927 | 0.000438 | -7.9E-05 | 0.000423 | 3.771E-07 |
| P12 | 0.155858 | 0.022748 | -0.04178 | 0.000437 | 0.000135 | -0.00055 | 5.104E-07 |

**Table 7.** Force and displacement at 12 points of the left first molar when the load is applied at the origin of force D

| | von Mises stress (MPa) | Maximal principal stress (MPa) | Minimal principal stress (MPa) | Displacement in x axis (mm) | Displacement in y axis (mm) | Displacement in z axis (mm) | $x^2+y^2+z^2$ |
|---|---|---|---|---|---|---|---|
| P1 | 0.02461 | 0.01494 | -0.01345 | -0.00123 | -0.00016 | -4.3E-05 | 1.535E-06 |
| P2 | 0.00734 | 0.00722 | -0.00024 | -0.00123 | -0.00072 | 0.00079 | 2.657E-06 |
| P3 | 0.00755 | 0.00132 | -0.00681 | -0.00158 | -0.00013 | -0.00014 | 2.538E-06 |
| P4 | 0.00561 | 0.00022 | -0.00549 | -0.00123 | 0.000507 | -0.00102 | 2.814E-06 |
| P5 | 0.00362 | 0.00137 | -0.0027 | -0.0009 | -0.00013 | -2.1E-05 | 8.211E-07 |
| P6 | 0.14375 | 0.07037 | -0.09508 | -0.00079 | -2.8E-05 | -0.00016 | 6.475E-07 |
| P7 | 0.05682 | -0.0123 | -0.07321 | -0.00058 | 0.000559 | -0.00102 | 1.695E-06 |
| P8 | 0.06528 | 0.03973 | -0.03561 | -0.00033 | -6.8E-05 | -1.8E-05 | 1.162E-07 |
| P9 | 0.05358 | 0.06462 | 0.005975 | -0.00056 | -0.00062 | 0.000789 | 1.322E-06 |
| P10 | 0.13077 | 0.13986 | -0.15153 | -0.00029 | -2.8E-07 | -0.00012 | 9.721E-08 |
| P11 | 0.21655 | 0.02441 | -0.02692 | 0.000399 | -4.3E-05 | 0.000328 | 2.688E-07 |
| P12 | 0.14158 | 0.0209 | -0.03883 | 0.000398 | 0.000152 | -0.00056 | 4.933E-07 |

talization, and group distalization. Compared to the distalization devices currently in use, our device is small in size and has a diminished foreign body sensation. Furthermore, the traction force is tunable by adjusting the length of the spring coil and spring compression.

Finite element analysis provides an effective approach for studying stress distribution in non-homogeneous materials with irregular geometric forms. Generally, materials are simplified in FEM by presuming them to be linearly elastic, homogeneous, and isotropic. The teeth and alveolar bones in our FEM were also presumed homogeneous, isotropic and linearly elastic material according to the literature [11, 13]. In the current study, we built the FEM for the upper first molar using CAD to evaluate force distribution and displacement of the upper canine, the first and second premolar and the first molar. Yoshida et al. [14] investigated displacement of teeth using the FEM without consideration of the actual measurements of the bracket and archwire. We built separate models for the alveolar bones, the periodontal membrane and the teeth, which have different elastic moduli and Poisson's ratios. Displacement restraint only limited alveolar bone movements and therefore, the movement of teeth can be indicated by the movement of the periodontal membrane.

Our 2D FEM and mechanical analysis of the sliding rod microscrew implantation device

revealed that, both horizontally and vertically, the traction force causing distalization of the first molar decreased when the spring coil moved down the L shaped sliding rod. Additionally, the mandible exhibited a trend for switch to clockwise rotation from counterclockwise rotation. It has been shown that the center of rotation changes by how the force is applied and the strength of the applied force [15]. The closer the distance to the center of the rotation of the tooth is, the smaller the displacement in the x, y and z axis is. By calculating the sum of $x^2+y^2+z^2$, we can identify the point closest to the center of rotation. Our 3D FEM showed that across all the five anchorage sites, P10 is closest to the center of rotation followed by P8, suggesting that P10 at the branching point of the root of the molar was closer to the center of rotation. The data from the 3D FEM suggests that though the sliding rod microscrew implantation device causes distalization of the upper first molar and the entire dental arch, the center of rotation remains stable.

Our 3D FEM analysis revealed distomedial displacement of the upper first molar when the the sliding rod microscrew implantation device caused distalization of the molar. When the origin of force moved down the sliding road, P4, P7, and P12 moved towards the palatal surface while P2, P9, and P11 moved toward the buccal surface. The movement causes the rotation of the first molar. When each point on the first molar exhibits distomedial displacement, the movement towards the palatal surface is greater than that towards the buccal surface. Guo et al. [16] also found horizontal rotation of the first molar, but in a different direction from that in our FEM, which may be due to different devices in the two studies. When the origin of force changed from A to D, the 12 points on the surface of the first molar mostly turned negative, indicating that they were pushed downward instead of being stretched, which is consistent with the findings from our mechanical analysis. We also found that P4, P7, and P12 displacement remained negative in the z axis while P2, P9, and P11 displacement remained positive in the z axis, indicating that the crown of the first molar remained tilted medioproximally and underwent stretching and depression in the mid sagittal plane. This may provide an explanation that the first molar experienced 3 times greater force in the x axis than the y axis.

Our 2D and 3D FEM analysis of the sliding rod microscrew implantation device has provided consistent delineation of force distribution and displacement of the upper canine, the first and second premolar and the first molar. However, this was achieved at the expense of simplification of material properties and meshing. In addition, boundary restraints were applied. These conditions differ sharply from actual clinical scenarios. The biomechanical properties of the sliding rod microscrew implantation device need to be further investigated in animal models and humans before it is used clinically. In conclusion, we have demonstrated that our sliding rod microscrew implantation device causes distalization of the upper first molar as well as group distalization. These findings support further exploration for the use of the sliding rod microscrew implants as an anchorage for group distal movement of the teeth of patients with mandibular prognathism.

## Acknowledgements

This study was funded by the Clinical Support of PLA General Hospital (2014FC-SXYY-1003) and the Capital's Special Health Development Research (2014-4-5022).

## Disclosure of conflict of interest

None.

**Address correspondence to:** Dr. Xianglong Zeng, Department of Orthodontics, School of Stomatology of Peking University, 22 South Venue of ZhongGuan Village, Haidian District, Beijing, China. Tel: +8601062179977-2350; Fax: +8601062179977-2350; E-mail: zengxianglong@sina.com; Dr. Yanfeng Li, Department of Stomatology, First Affiliated Hospital of Peoples Liberation Army General Hospital, 51 Fuchengmen Road, Haidian District, Beijing, China. Tel: +8601066867496; Fax: +8601066867491; E-mail: m.god@yeah.net

## References

[1] Zeng XL. Modern orthodontics treatment manual. Beijing: Beijing Medical University Press; 2000.

[2] Nevzatoglu S and Kucukkeles N. Long-term results of surgically-assisted maxillary protraction. Aust Orthod J 2014; 30: 19-31.

[3] Li JR. Technical application of a novel implant anchorage technology. Chinese Journal of Oral Orthodontics 2009; 16: 38-44.

[4] Lim JK, Jeon HJ and Kim JH. Molar distalization with a miniscrew-anchored sliding jig. J Clin Orthod 2011; 45: 368-377.
[5] Wu JP, Zhao ZH. Review on the clinical application of molar distallization techniques. International Journal of Stomatology 2008; 35: 336.
[6] Zhang HJ. Ji GP, Shen G. A clinical study on effects of distalization of whole upper arch in borderline Class II malocclusion using microscrew anchorages in inferiozygomatic area. Shanghai Journal of Stomatology 2013; 22: 310-315.
[7] Park HS, Lee SK, Know OW. Group distal movement of teeth using microscrew implant anchorage. Angle Orthod 2005; 75: 602-609.
[8] Kyung SH, Lee JY, Shin JW, Hong C, Dietz V and Gianelly AA. Distalization of the entire maxillary arch in an adult. Am J Orthod Dentofacial Orthop 2009; 135: S123-132.
[9] Li S, Duan YZ. Effects of Maxillary Molar Distalization on Dental and Maxillofacial Vertical Dimension [Master's thesis]: The Fourth Military Medical University; 2006.
[10] Bowman SJ. Class II combination therapy. J Clin Orthod 1998; 32: 611-620.
[11] Basciftci FA, Korkmaz HH, Iseri H and Malkoc S. Biomechanical evaluation of mandibular midline distraction osteogenesis by using the finite element method. Am J Orthod Dentofacial Orthop 2004; 125: 706-715.
[12] Ueno S, Motoyoshi M, Mayahara K, Saito Y, Akiyama Y, Son S and Shimizu N. Analysis of a force system for upper molar distalization using a trans-palatal arch and mini-implant: a finite element analysis study. Eur J Orthod 2013; 35: 628-633.
[13] Zhou Z, Chen W, Shen M, Sun C, Li J and Chen N. Cone beam computed tomographic analyses of alveolar bone anatomy at the maxillary anterior region in Chinese adults. J Biomed Res 2014; 28: 498-505.
[14] Yoshida N, Jost-Brinkmann PG, Koga Y, Mimaki N and Kobayashi K. Experimental evaluation of initial tooth displacement, center of resistance, and center of rotation under the influence of an orthodontic force. Am J Orthod Dentofacial Orthop 2001; 120: 190-197.
[15] Tai K, Hotokezaka H, Park JH, Tai H, Miyajima K, Choi M, Kai LM and Mishima K. Preliminary cone-beam computed tomography study evaluating dental and skeletal changes after treatment with a mandibular Schwarz appliance. Am J Orthod Dentofacial Orthop 2010; 138: 262.e1-262.e11; discussion 262-3.
[16] Guo J, Duan YZ. The clinical study of distalizing upper molar by implant anchorage [Master's thesis]: The Fourth Military Medical University; 2006.